nature neuroscience

Optogenetic silencing strategies differ in their effects on inhibitory synaptic transmission

Joseph V Raimondo, Louise Kay, Tommas J Ellender & Colin J Akerman

Optogenetic silencing using light-driven ion fluxes permits rapid and effective inhibition of neural activity. Using rodent hippocampal neurons, we found that silencing activity with a chloride pump can increase the probability of synaptically evoked spiking after photoactivation; this did not occur with a proton pump. This effect can be accounted for by changes to the $GABA_A$ receptor reversal potential and demonstrates an important difference between silencing strategies.

Multiple strategies have emerged for rapidly silencing the activity of neurons, all of which use the flux of various ion species to control the membrane potential and resistance[1–3]. Given that the same ion species are used by neurotransmitter receptors and channels, an important consideration is how optical silencing tools may interact with endogenous signaling systems[4–6]. A potential benefit of this approach is that it also offers the opportunity to use light-activated proteins as ion modulators with which to investigate cellular function[7]. The two most successful silencing strategies have used light-driven chloride pumps, which move Cl^- into the cell[2,8], and proton pumps, which move protons out of the cell and thereby generate a hyperpolarizing effect[9,10]. We found that, although a light-driven inward Cl^- pump[11] (*Natronomonas pharaonis* halorhodopsin, eNpHR3.0 or NpHR) and a light-driven outward H^+ pump[9] (Archaerhodopsin-3 from *Halorubrum sodomense*, Arch) are both effective silencers of neural activity in mammalian neurons, they differed in terms of their effect beyond the light-activation period. NpHR, unlike Arch, caused changes in the reversal potential of the $GABA_A$ receptor (E_{GABAA}), which resulted in changes in synaptically evoked spiking activity in the period following light activation.

To compare the effects of optogenetic silencing strategies following synaptically evoked action potential activity, we performed cell-attached recordings from pyramidal neurons in the CA1 and CA3 regions of rat hippocampal organotypic brain slices, which had been biolistically transfected with either eNpHR3.0-EYFP (enhanced yellow fluorescent protein) or Arch-GFP. Postsynaptic spikes were elicited by brief electrical stimuli to the Schaffer collateral pathway. This stimulus recruited convergent monosynaptic and polysynaptic excitatory and inhibitory postsynaptic potentials, which exhibited mature properties at the time of our recordings (Online Methods and **Supplementary Figs. 1** and **2**). Synaptically evoked spike probability was measured before and after a 15-s period of laser activation (532 nm, mean intensity 19.4 ± 3.4 mW mm^{-2}). Separate whole-cell recordings confirmed that these laser settings resulted in robust hyperpolarizing photocurrents in both NpHR- and Arch-expressing neurons, which were similar in amplitude (mean NpHR photocurrent = 237 ± 46 pA, mean Arch photocurrent = 235 ± 40 pA; **Supplementary Fig. 3c**). The photocurrents exhibited fast onset and offset kinetics, as has been shown previously[10,12] (**Supplementary Fig. 3a**,**b**), and were effective at inhibiting spiking activity during the period in which the laser was on (see below). However, cells responded differently to synaptic input in the period following light activation. In NpHR-expressing cells, the mean spike probability increased significantly from 0.37 ± 0.05 before laser activation to 0.82 ± 0.04 after laser activation (n = 10 cells, P = 0.00015, paired t test; **Fig. 1a**). The mean stimulus-evoked spike rate (measured over 200 ms) also increased from 1.9 ± 0.3 Hz before laser activation to 5.5 ± 0.9 Hz after laser activation (P = 0.005, paired t test). This was in contrast with recordings from Arch-expressing cells, which had a comparable spike probability before and after laser activation, even when the highest laser intensities were used (range of 7.9–76.1 mW mm^{-2}; **Fig. 1b**). In Arch-expressing cells, the spike probability before laser activation was 0.43 ± 0.04 and the equivalent measure was 0.45 ± 0.05 after laser activation (n = 12 cells, P = 0.74, paired t test; **Fig. 1b**). The mean stimulus-evoked spike rate was also stable for Arch-expressing cells at 2.15 ± 0.2 Hz before laser activation and 2.3 ± 0.3 Hz after laser activation (P = 0.64, paired t test).

One explanation for the difference between the two light-activated pumps is that NpHR activation results in an accumulation in intracellular Cl^-, which then has sustained effects on inhibitory synaptic transmission[4–6]. $GABA_A$ receptors ($GABA_A$Rs) are primarily permeable to Cl^- ions (approximately fourfold more permeable to Cl^- than bicarbonate), and strong $GABA_A$R activation is known to result in intracellular Cl^- accumulation and a collapse in the Cl^- gradient (but not the bicarbonate gradient), which causes depolarizing shifts in E_{GABAA}[13,14]. Using organotypic hippocampal slices and acute hippocampal slices, we confirmed that Cl^- influxes associated with $GABA_A$R activation can result in substantial depolarizing shifts in E_{GABAA} (**Supplementary Fig. 1**). As a first test of whether NpHR has sustained effects on GABAergic transmission, we performed current-clamp recordings using the perforating agent gramicidin, which preserves intracellular Cl^-. Under these conditions, a brief somatic puff of GABA (100 μM) normally generated a hyperpolarizing response, but when the same puff was delivered after a period of NpHR activation, a depolarizing response and action potentials were generated (n = 5 cells; **Fig. 1c**).

We then performed a series of voltage-clamp experiments to compare E_{GABAA} before and after light activation. Resting E_{GABAA} values did not differ between the NpHR-expressing (mean of –68.7 ± 1.2 mV, n = 18 cells) and Arch-expressing (mean of –68.5 ± 1.0 mV, n = 13 cells) neurons (P = 0.89, t test). However, NpHR activation for 15 s consistently changed the amplitude and/or polarity of $GABA_A$R currents, such

Department of Pharmacology, Oxford University, Oxford, UK. Correspondence should be addressed to C.J.A. (colin.akerman@pharm.ox.ac.uk).

Received 3 February; accepted 21 May; published online 24 June 2012; doi:10.1038/nn.3143

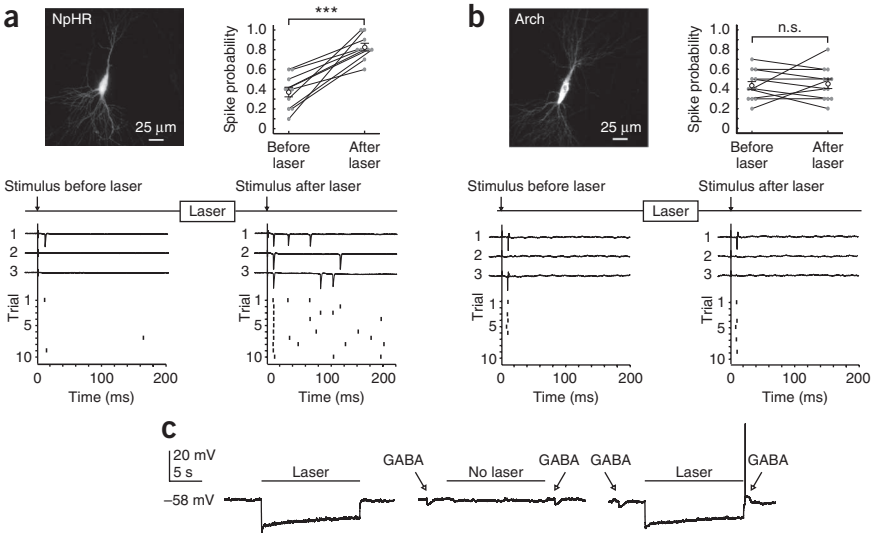

Figure 1 Optogenetic silencing strategies differ in their effects on synaptically evoked spiking activity. (**a**) Top left, confocal image of a CA3 pyramidal neuron expressing eNpHR3.0-EYFP (NpHR). Bottom, cell-attached recordings from this cell showing synaptically evoked spiking before (left) and after (right) NpHR activation (15 s, 532 nm, 7.9 mW mm^{-2}). Spike probability was set to approximately 0.4 before laser activation (measured over ten trials). The before stimulus was delivered 1,250 ms before laser onset and the after stimulus was delivered 250 ms after laser offset. Top right, spike probability for NpHR cells ($n = 10$; error bars, s.e.m.; $^{***}P < 0.001$). (**b**) Top left, a CA3 pyramidal neuron expressing Arch-GFP (Arch). Bottom, cell-attached recordings from this cell showing synaptically evoked spiking before (left) and after (right) Arch activation (15 s, 532 nm, 76.1 mW mm^{-2}). Top right, spike probability for Arch cells ($n = 12$; n.s., nonsignificant, $P = 0.74$). Presented as in **a**. (**c**) Perforated-patch current-clamp recording from an NpHR-expressing neuron. Laser activation (10.9 mW mm^{-2} for 15 s) evoked a sustained hyperpolarizing response (left). In the absence of laser activation, GABA puffs elicited hyperpolarizing responses (middle). The same GABA puff generated a depolarizing response and action potential when delivered 250 ms after laser activation (right).

that $GABA_AR$ currents that were outward before laser activation often became strong inward currents after laser activation (measured 250 ms after laser offset; **Fig. 2a**), consistent with the light-driven accumulation of intracellular Cl^-. Arch-expressing cells, by contrast, showed stable $GABA_AR$ currents across a range of photocurrents (**Fig. 2b**).

The effect on $GABA_AR$ currents was quantified by estimating E_{GABAA} for individual GABA puffs and relating this to the size of the photocurrent (Online Methods and **Fig. 2c**). This revealed a strong positive correlation between the size of the NpHR photocurrent and the change in E_{GABAA} ($r = 0.70$, $P < 10^{-19}$, Pearson correlation). The slope of the linear fit for the NpHR data indicated an 8.8-mV shift in E_{GABAA} per 100 pA of mean photocurrent (**Fig. 2d**). Mean NpHR photocurrents between 90 and 400 pA, which effectively blocked spiking activity evoked by somatic positive current injection (Online Methods and **Fig. 2a**,**b**), generated an average E_{GABAA} shift of 19.7 ± 1.7 mV ($P < 10^{-14}$, *t* test). Modest mean NpHR photocurrents between 25 and 50 pA also generated a significant change in E_{GABAA} of 4.8 ± 1.0 mV ($P = 0.0004$, *t* test). In contrast, Arch-expressing cells exhibited much more stable E_{GABAA} across a range of photocurrents (**Fig. 2d**); the slope of the linear fit for the Arch data was –0.4 mV per 100 pA of mean photocurrent, with a small negative correlation between Arch photocurrent and the change in E_{GABAA} ($r = -0.2213$, $P = 0.023$, Pearson correlation). The slopes of the linear fits for the two optical silencers were highly statistically different ($P < 0.0001$, analysis of covariance).

Our measurements of the effects of NpHR photocurrents on E_{GABAA} are consistent with a model that we generated of Cl^- homeostasis mechanisms, based on realistic cell parameters (**Supplementary Fig. 4**). To determine whether the effect of NpHR photocurrents on E_{GABAA} is evident in different experimental preparations, we examined excitatory neurons from mice that had received *in vivo* viral delivery of one of the optical silencers via injections into the hippocampus (Online Methods). Neurons recorded in acute hippocampal slices showed a strong relationship between NpHR photocurrent and change in E_{GABAA} ($r = 0.50$, $P < 0.0001$, Pearson correlation, linear fit of 8.9 mV per 100 pA of photocurrent, $n = 7$ cells; **Fig. 2d** and **Supplementary Fig. 5a**), which was statistically indistinguishable from neurons with plasmid-driven NpHR expression in organotypic slices ($P = 0.89$, analysis of covariance). Given that measurements of E_{GABAA} made after a Cl^- load reflect the rate of endogenous recovery mechanisms, this indicates that NpHR photocurrents can overwhelm Cl^- extrusion capacity to a similar degree in organotypic and acute slices (**Supplementary Fig. 1**). Neurons infected with Arch-expressing virus showed stable E_{GABAA} across a range of photocurrents ($r = -0.07$, $P = 0.68$, Pearson correlation, linear fit of –0.2 mV per 100 pA of photocurrent, $n = 6$ cells; **Fig. 2d** and **Supplementary Figs. 5b** and **6**).

To further characterize the timescale of the effects of NpHR activation, we estimated E_{GABAA} at different times after laser activation. The rate of recovery of E_{GABAA} had a time constant of 14.7 ± 3.2 s, on average (**Fig. 2e** and **Supplementary Fig. 5c**,**d**), which is similar to that seen after increases in intracellular Cl^- generated by $GABA_AR$ activation[13,14]. Finally, varying the duration of the light-activation period revealed that changes in E_{GABAA} were closely related to the duration of the photocurrent and were evident for relatively short photocurrents (**Fig. 2f** and **Supplementary Fig. 5e**,**f**). Significant positive shifts in E_{GABAA} were detected following photocurrents of just 500-ms duration (2.41 ± 0.5 mV change in E_{GABAA}, $P = 0.0014$, *t* test) and revealed an incremental relationship with longer photocurrents. Finally, the NpHR-mediated shift in E_{GABAA} affected cells with different resting E_{GABAA}, consistent with endogenous Cl^- regulation mechanisms being overwhelmed (**Supplementary Fig. 7**).

Thus, silencing neural activity with a Cl^- pump, but not a H^+ pump, can alter GABAergic synaptic transmission beyond the period of silencing and in a manner that alters network excitability. The effects on E_{GABAA} were directly related to the size and duration of the Cl^- photocurrent, with brief, small photocurrents generating the smallest shifts in E_{GABAA}. This can account for previous findings that an earlier version of NpHR, which generates smaller photocurrents, did not affect GABAergic transmission[6]. For larger photocurrents, which offer more effective silencing[11], the amplitude and duration of the photocurrent had a critical effect on the degree of E_{GABAA} shift. In contrast, inhibitory photocurrents of comparable amplitude and duration achieved via a proton pump did not affect GABAergic synaptic transmission. Our data are consistent with reports of depolarizing shifts in the driving force for $GABA_ARs$ in mature neurons, which result from an overwhelming of endogenous Cl^- homeostasis mechanisms while bicarbonate

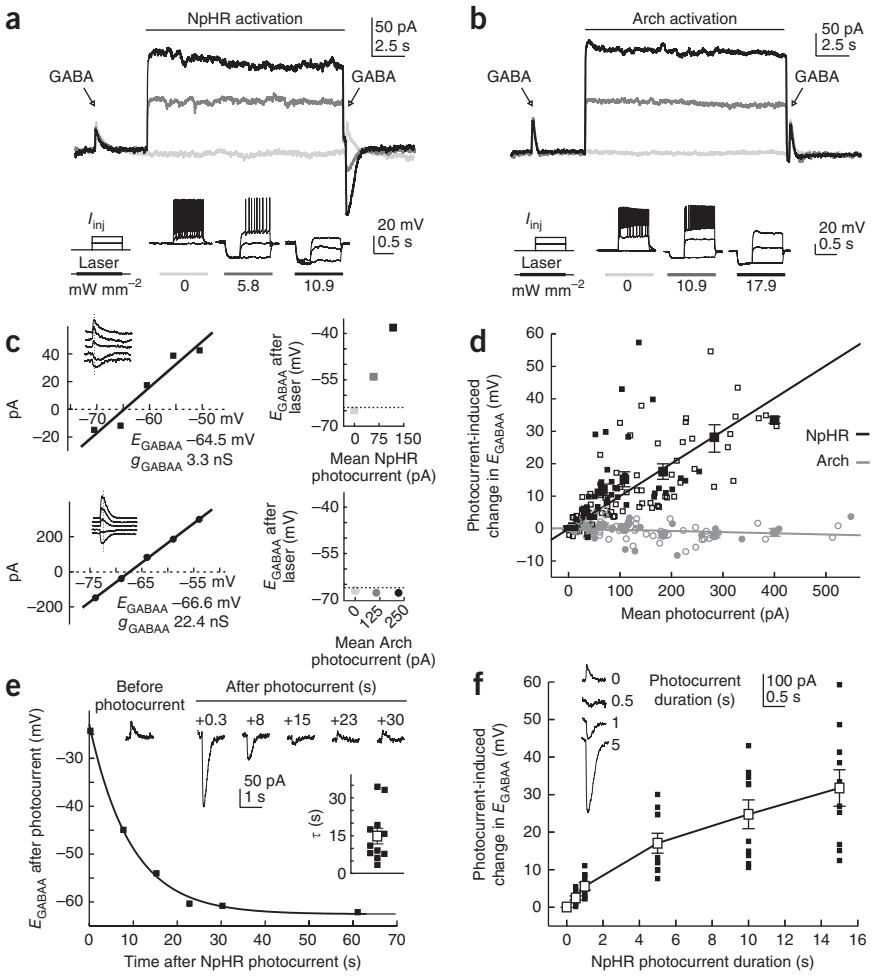

Figure 2 A light-activated Cl^- pump, but not a H^+ pump, causes a sustained change in GABAergic transmission. (**a**) Top, gramicidin perforated-patch voltage-clamp recording from a neuron expressing eNpHR3.0-EYFP. $GABA_AR$ currents measured before and after NpHR activation using three different laser intensities: zero (light gray), intermediate (dark gray) and high (black). Bottom, laser intensities were selected by assessing their effectiveness in silencing spikes evoked by somatic current injection in current clamp (see Online Methods). (**b**) Recordings from a neuron expressing Arch-GFP, presented as in **a**. (**c**) Estimation of the effects of photocurrents on E_{GABAA} for the NpHR cell in **a** (top) and Arch cell in **b** (bottom). $GABA_AR$ *I-V* plots (left) were used to calculate the resting E_{GABAA} and $GABA_AR$ conductance (g_{GABAA}), which were then used to estimate E_{GABAA} for individual GABA puffs delivered after different mean photocurrents (right; symbol colors correspond to data in **a**,**b**). (**d**) Changes in E_{GABAA} associated with photocurrents. Small empty symbols, data from organotypic hippocampal slices. Small filled symbols, data from acute hippocampal slices. Large symbols with error bars (s.e.m.), combined population averages. (**e**) Traces from a representative NpHR-expressing neuron showing $GABA_AR$ currents recorded at different times after the photocurrent, on different trials. E_{GABAA} versus time after photocurrent is plotted for this cell; recovery is fitted by a single-exponential function. Inset, distribution of time constants (τ) of E_{GABAA} recovery for all NpHR-expressing cells. (**f**) Traces from a representative NpHR-expressing neuron showing $GABA_AR$ currents recorded after photocurrents of different durations. Plot illustrates the change in E_{GABAA} as a function of photocurrent duration for all NpHR-expressing cells. Error bars, s.e.m.

(and therefore proton) gradients are maintained[13,14]. This is believed to be because whereas only transport mechanisms have been described for Cl^-, bicarbonate and pH gradients are more stably maintained by a combination of transport mechanisms and a series of efficient intracellular and extracellular buffering mechanisms[13,15]. Our observations therefore establish an important difference between optical silencing strategies, which are relevant to *ex vivo* and *in vitro* experiments, and may be helpful in interpreting *in vivo* experiments. Our findings also highlight the usefulness of light-activated proteins as ion modulators, which will be invaluable for exploring the role of ion species in synaptic transmission, development and pathology.

METHODS

Methods and any associated references are available in the online version of the paper.

Note: Supplementary information is available in the online version of the paper.

ACKNOWLEDGMENTS

We thank P. Bolam (Oxford University) for resources, and K. Deisseroth (Stanford University) and E. Boyden (Massachusetts Institute of Technology) for DNA constructs. We also thank G. Miesenböck, D. Kätzel and B. Richards for comments. Supported by a grant from the Medical Research Council (G0601503); research leading to these results received funding under the European Community's Seventh Framework Programme (FP7/2007-2013).

AUTHOR CONTRIBUTIONS

J.V.R. and C.J.A. designed the research. J.V.R., T.J.E. and L.K. performed the experiments. J.V.R. and C.J.A. analyzed the data. J.V.R. and C.J.A. wrote the paper.

COMPETING FINANCIAL INTERESTS

The authors declare no competing financial interests.

Published online at http://www.nature.com/doifinder/10.1038/nn.3143.
Reprints and permissions information is available online at http://www.nature.com/reprints/index.html.

1. Boyden, E.S., Zhang, F., Bamberg, E., Nagel, G. & Deisseroth, K. *Nat. Neurosci.* **8**, 1263–1268 (2005).
2. Zhang, F. *et al. Nature* **446**, 633–639 (2007).
3. Zemelman, B.V., Lee, G.A., Ng, M. & Miesenböck, G. *Neuron* **33**, 15–22 (2002).
4. Gradinaru, V. *et al. J. Neurosci.* **27**, 14231–14238 (2007).
5. Fenno, L., Yizhar, O. & Deisseroth, K. *Annu. Rev. Neurosci.* **34**, 389–412 (2011).
6. Tønnesen, J., Sørensen, A.T., Deisseroth, K., Lundberg, C. & Kokaia, M. *Proc. Natl. Acad. Sci. USA* **106**, 12162–12167 (2009).
7. Gourine, A.V. *et al. Science* **329**, 571–575 (2010).
8. Han, X. & Boyden, E.S. *PLoS ONE* **2**, e299 (2007).
9. Chow, B.Y. *et al. Nature* **463**, 98–102 (2010).
10. Mattis, J. *et al. Nat. Methods* **9**, 159–172 (2012).
11. Gradinaru, V. *et al. Cell* **141**, 154–165 (2010).
12. Madisen, L. *et al. Nat. Neurosci.* **15**, 793–802 (2012).
13. Staley, K.J. & Proctor, W.R. *J. Physiol. (Lond.)* **519**, 693–712 (1999).
14. Wright, R., Raimondo, J.V. & Akerman, C.J. *Neural Plast.* **2011**, 728395 (2011).
15. Chesler, M. *Physiol. Rev.* **83**, 1183–1221 (2003).

ONLINE METHODS

Slice preparation. Rat organotypic hippocampal slice cultures were prepared using methods similar to those described previously[16]. Briefly, 350-μm-thick hippocampal slices were cut from 7-d-old male Wistar rats, placed onto Millicell-CM membranes and maintained in culture media containing 25% Earle's balanced salt solution (vol/vol), 49% MEM (vol/vol), 25% heat-inactivated horse serum (vol/vol), 1% B27 (vol/vol, Invitrogen) and 6.2 g l^{-1} glucose. Neurons were biolistically transfected after 5–6 d *in vitro* using a Helios Gene Gun in accordance with the manufacturer's instructions (Bio-Rad). The target DNA was either pLenti-hSyn-eNpHR3.0-EYFP (eNpHR3.0 fused to EYFP and driven by the human synapsin 1 promoter, *SYN1*)[11], generously provided by K. Deisseroth (Stanford University) or FCK-Arch-GFP (Arch fused to GFP and driven by the mouse α-CamKII promoter, *Camk2a*)[9], generously provided by E. Boyden (Massachusetts Institute of Technology). Recordings were performed 2–4 d post-transfection, which is equivalent to postnatal days 14–17. Previous work in rat hippocampus has shown that E_{GABAA} reaches mature levels in the first two postnatal weeks[17] and recordings from rat organotypic hippocampal slices have confirmed that GABAergic[18] and glutamatergic[19] synaptic transmission are mature at these stages (**Supplementary Figs. 1** and **2**).

Acute slices were prepared from 3–5-week-old male Wistar rats and 5–8-week-old CAMKII-cre mice (Jackson Laboratory). Adeno-associated virus serotype 2 (AAV2) carrying eNpHR3.0-EYFP or Arch-GFP was injected into the hippocampus of the CAMKII-cre mice between postnatal days 14 and 21. Typical coordinates from Bregma for injections in ventral hippocampus were 3.1 mm lateral, 2.7 mm posterior and 3.25–2.25 mm ventral to the surface of brain. Viral DNA included the *loxP*-flanked sequence for eNpHR3.0-EYFP driven by the human elongation factor 1a promoter (*EEF1A1*) or the *loxP*-flanked sequence for Arch-GFP driven by the cytomegalovirus early enhancer element and chicken beta-actin (*CAG*) promoter. Typical titers were ~10^{12} IU ml^{-1}. Injection volumes were 500 nl. After allowing 2–4 weeks for expression, we prepared acute horizontal hippocampal slices (350–400 μm thick).

The DNA constructs used to drive expression of the optical silencers were selected because they achieve good levels of neuronal expression, without toxicity effects, and are widely used in the field[9,11,20,21]. The experimental design compared the silencers by matching for photocurrent amplitude, which equates to the strength of the optical silencing, and therefore controlled for functional expression levels. In addition, there was no significant difference across the constructs in terms of the maximum photocurrent evoked ($P = 0.47$, ANOVA; maximum evoked photocurrent was 236.4 ± 25.5 pA, 244.7 ± 49.6 pA, 167.8 ± 26.0 pA and 192.9 ± 58.5 pA for NpHR in organotypics, Arch in organotypics, NpHR in acutes and Arch in acutes, respectively). Similarly, there was no significant difference across constructs in terms of resting E_{GABAA}, indicating that endogenous ion homeostasis mechanisms were comparable ($P = 0.64$, ANOVA; resting E_{GABAA} was −67.3 ± 1.7 mV, −68.4 ± 1.2 mV, −69.8 ± 1.8 mV and −69.5 ± 1.2 mV for NpHR in organotypics, Arch in organotypics, NpHR in acutes and Arch in acutes, respectively).

Electrophysiology. Hippocampal slices were transferred to the recording chamber and continuously superfused with 95% O_2 and 5% CO_2 oxygenated artificial cerebrospinal fluid, heated to 30 °C (ref. 22). For cell-attached recordings, 2-chloroadenosine (2 μM) was added to the artificial cerebrospinal fluid to reduce spontaneous activity. For perforated-patch recordings, glutamatergic receptors and $GABA_B$Rs were blocked with kynurenic acid (2 mM) and CGP55845 (5 μM), respectively. Neurons in the pyramidal cell layer of the CA1 and CA3 regions of the hippocampus were targeted for recording. For cell-attached recordings, pipettes (3–7-MΩ tip) were back-filled with an internal solution composed of 130 mM potassium gluconate, 10 mM NaCl, 0.1333 mM $CaCl_2$ 2 mM $MgCl_2$, 1 mM EGTA, 4 mM KCl and 10 mM HEPES. For gramicidin perforated-patch recordings, pipettes were filled with a high KCl internal solution whose composition was 135 mM KCl, 4 mM Na_2ATP, 0.3 mM NaGTP, 2 mM $MgCl_2$ and 10 mM HEPES. Gramicidin (Calbiochem) was dissolved in dimethylsulfoxide to achieve a stock solution of 4 mg ml^{-1}. Fresh stock solution was prepared daily and diluted in internal solution immediately before experimentation to achieve a final concentration of 80 μg ml^{-1}. The osmolarity of internal solutions was adjusted to 290 mOsM and the pH was adjusted to 7.38 with KOH.

Spike probability was assessed from recordings in the loose cell-attached patch configuration (50–150 MΩ). Synaptically evoked spikes were triggered via a bipolar stimulating electrode placed in stratum radiatum, 300–400 μm from the recorded cell[23]. Stimulus intensity was set such that spikes (detected during a 200-ms window immediately after the stimulus) were evoked with a probability of approximately 0.4 before laser activation (that is, four of ten trials resulted in at least one spike). The before laser stimulus was delivered 1,250 ms before laser onset and the after laser stimulus was delivered 250 ms after laser offset. We tested for post-inhibitory rebound spikes by examining responses to 15 s of laser activation in the absence of a synaptic stimulus. Consistent with previous reports[24], cells showing rebound spikes were rare (7 of 54) and were not included in the analyses. Perforated-patch recordings were started once the access resistance had stabilized between 20–50 MΩ (mean R_a of ~35 MΩ). For all experiments, online series resistance correction of 70% was used. Recordings were made using an Axopatch 700A amplifier and data were acquired using Clampex software (Molecular Devices). All values reported from voltage-clamp recordings were corrected offline for the liquid junction potential (4.2 mV) between the intracellular and extracellular solution.

$GABA_A$Rs were activated by delivering short puffs of GABA (100 μM) in the presence of glutamate receptor blockers and $GABA_B$R blockers (see above). The agonist was applied via a patch pipette positioned close to the soma and connected to a picospritzer. To calculate resting E_{GABAA} and g_{GABAA}, we measured $GABA_A$R currents at five different holding potentials (5-mV intervals around the resting membrane potential) in response to a GABA puff. A minimum of 30 s was allowed before each puff to allow full recovery of Cl^- homeostasis[13,14,25]. The peak $GABA_A$R current was plotted as a function of holding potential to generate a current-voltage curve (**Fig. 2c**), from which resting E_{GABAA} was defined as the *x* intercept value and the peak $GABA_A$R conductance (g_{GABAA}) as the slope. To measure the effect of photocurrents on E_{GABAA}, it was important to estimate E_{GABAA} from single $GABA_A$R currents. To achieve this, we calculated resting E_{GABAA} and g_{GABAA} before each experiment (as described above) and used these values to estimate E_{GABAA} for a single $GABA_A$R current by assuming a constant g_{GABAA} across GABA puffs and solving the equation $GABA_A$R current = g_{GABAA}(Holding potential − E_{GABAA}).

The GABA puffs enabled us to consistently activate $GABA_A$Rs on the somatic compartment of the recorded neuron, where the perforated-patch clamp recordings have the best control of membrane potential, thus optimizing our measurements of E_{GABAA}. The peak g_{GABAA} was not statistically different between NpHR-expressing cells (9.70 ± 1.69 nS, $N = 26$) and Arch-expressing cells (9.27 ± 1.76 nS, $N = 21$; $P = 0.86$, *t* test). In addition, there was no correlation between the peak g_{GABAA} and the photocurrent-induced shift in E_{GABAA} for either NpHR-expressing cells ($r = 0.02$, $P = 0.90$, Pearson correlation) or Arch-expressing cells ($r = 0.03$, $P = 0.89$, Pearson correlation).

Data analysis was performed using custom-made programs in the MATLAB environment (MathWorks). Some statistical analysis was also performed using GraphPad Prism version 5.00 (GraphPad Software). Data are reported as mean ± s.e.m.

Photoactivation of NpHR and Arch was achieved via a diode-pumped solid-state (532-nm peak wavelength) laser (Shanghai Laser Optic Century). The laser was coupled to a 1,000-μm diameter mulitimode optic fiber via a collimating lens (Thorlabs). The tip of the optic fiber was positioned at an image plane in the microscope in the center of the optical axis, and directed into the objective lens via a dichroic mirror. This resulted in a spot of light at the brain slice whose diameter was 195 μm, assuming zero tissue scattering. Laser stimulation elicited photocurrents in both Arch- and NpHR-expressing cells of comparable size (**Supplementary Fig. 3c**) and kinetics (**Supplementary Fig. 3a**,**b**) as those reported previously[9,10]. Consistent with published work, both constructs appeared to have no observable toxic effects on the tissue concerned[9,10]. For the gramicidin recordings, functionally relevant laser intensities were defined by assessing the ability of the photocurrents to inhibit spiking in response to somatic current injections via the recording pipette (**Fig. 2**). First, we injected a range of current steps in current clamp (1-s duration) without any laser activation, from which we defined a threshold somatic current (the minimum current that evoked spiking, mean of 112 ± 25 pA, which generated a mean spike rate of 4.1 ± 0.8 Hz, $n = 12$) and a strong somatic current (twice the amplitude of the threshold current, mean of 224 ± 50 pA, which generated a mean spike rate of 13.3 ± 2.6 Hz). An intermediate laser intensity produced the minimum mean photocurrent (104 ± 17 pA, range = 40–230 pA) required to inhibit all spiking activity in response to the threshold somatic current.

doi:10.1038/nn.3143

A higher laser intensity produced the minimum mean photocurrent (207 ± 35 pA, range = 90–400 pA) required to inhibit all spiking in response to the strong somatic current injection.

16. Stoppini, L., Buchs, P.A. & Muller, D. *J. Neurosci. Methods* **37**, 173–182 (1991).
17. Tyzio, R., Holmes, G.L., Ben-Ari, Y. & Khazipov, R. *Epilepsia* **48**, 96–105 (2007).
18. Streit, P., Thompson, S.M. & Gähwiler, B.H. *Eur. J. Neurosci.* **1**, 603–615 (1989).
19. De Simoni, A., Griesinger, C.B. & Edwards, F.A. *J. Physiol. (Lond.)* **550**, 135–147 (2003).
20. Olsen, S.R., Bortone, D.S., Adesnik, H. & Scanziani, M. *Nature* **483**, 47–52 (2012).
21. Cardin, J.A. *J. Physiol. Paris* published online: doi:10.1016/j.jphysparis.2011.09.005 (19 September 2011).
22. Hartmann, A.M. & Nothwang, H.G. *BMC Res. Notes* **4**, 526 (2011).
23. Pouille, F. & Scanziani, M. *Science* **293**, 1159–1163 (2001).
24. Ascoli, G.A., Gasparini, S., Medinilla, V. & Migliore, M. *J. Neurosci.* **30**, 6434–6442 (2010).
25. Jin, X., Huguenard, J.R. & Prince, D.A. *J. Neurophysiol.* **93**, 2117–2126 (2005).